actuators

MDPI

Article

The Actuating Characteristics of Magnetorheological Fluids Subjected to Particle Sedimentation and Temperature Variation

Elliza Tri Maharani [1], Dong-Hoon Lee [2], Young-Jun Kim [3], Jong-Seok Oh [2,3,*] and Seung-Bok Choi [4,5,*]

[1] Department of Mechanical Engineering, Kongju National University, Cheonan 31080, Republic of Korea; a20220347@smail.kongju.ac.kr
[2] Department of Future Automotive Engineering, Kongju National University, Cheonan 31080, Republic of Korea; ehdgns6245@smail.kongju.ac.kr
[3] Department of Future Convergence Engineering, Kongju National University, Cheonan 31080, Republic of Korea; d20230046@smail.kongju.ac.kr
[4] Department of Mechanical Engineering, The State University of New York Korea (SUNY Korea), Incheon 21985, Republic of Korea
[5] Department of Mechanical Engineering, Industrial University of Ho Chi Minh City, Ho Chi Minh City 70000, Vietnam
* Correspondence: jongseok@kongju.ac.kr (J.-S.O.); seungbok.choi@sunykorea.ac.kr (S.-B.C.)

Abstract: Magnetorheological (MR) fluids are known for their controllable characteristics under the influence of magnetic fields and, hence, widely used as semi-active actuators for vibration control. Regardless of advantages such as fast response time and reversible property, MR fluids inevitably experience sedimentation caused by significant density mismatches between magnetic particles and carrier liquids. Moreover, the effect of the temperature on actuating characteristics is also one of the problems to be resolved for practical implementation. This study experimentally investigates the sedimentation behavior under various temperatures ranging from 25 to 70 °C using a multiguide-arm magnetic device that generates a uniform magnetic flux density across MR fluids. The sedimentation stability is then observed after 168 h at current inputs of 0, 1, and 2 A, respectively. Subsequently, the field-dependent rheological properties of MR fluids are evaluated using a rheometer and discussed, showing actuating capability, which depends on the viscosity, shear stress, and yield stress before (initial state) and after the sedimentation (sedimentation state). The field-dependent yield stresses, which directly represent the actuating force of the semi-active actuator, are specifically evaluated. Under the on-state condition (2 A) at a temperature of 70 °C, the yield stress decreased from 2.747 kPa (initial state) to 2.352 kPa (sedimentation state). By using this yield stress, the field-dependent damping force was evaluated, showing a decrement from 1672 N (initial state) to 1623 N (sedimentation state) at a velocity of 0.8 m/s. It is shown that the temperature causes the reduction of the actuating properties after the long-term operation. The insightful findings achieved in this work will provide useful information for the evaluation of actuating characteristics of smart MR fluids and the design of MR application systems subjected to particle sedimentation and temperature variation.

Keywords: MR fluids; semi-active actuator; actuating characteristics; particle sedimentation; temperature; magnetic field; rheological properties

Citation: Maharani, E.T.; Lee, D.-H.; Kim, Y.-J.; Oh, J.-S.; Choi, S.-B. The Actuating Characteristics of Magnetorheological Fluids Subjected to Particle Sedimentation and Temperature Variation. *Actuators* **2024**, *13*, 277. https://doi.org/10.3390/act13080277

Academic Editor: Janusz Gołdasz

Received: 24 June 2024
Revised: 20 July 2024
Accepted: 22 July 2024
Published: 24 July 2024

1. Introduction

Magnetorheological (MR) fluids are recognized as intelligent (or smart) materials whose rheological characteristics are easily influenced by an external magnetic field. It is known that the actuator utilizing MR fluids is semi-active since it controls only damping force by regulating the intensity of the magnetic field [1]. For this reason, MR fluids are widely found in controllable devices in many application sectors such as automotive (MR clutches, MR dampers, MR mounts, MR brakes) [2–5], seismic protection (MR dampers for building) [6], and material removal (surface precision machining) [7]. MR fluids' working

principle is divided into two conditions: on-state condition and off-state condition. The off-state condition is when MR fluids are not subjected to any influence of magnetic fields. In this state, MR fluids freely flow and act like Newtonian fluids. On the other hand, MR fluids under the influence of magnetic fields, act as Bingham plastic materials, which allow the iron particles to form chain formations in a solid state. Generally, carbonyl iron particles (CIP: most general magnetic particles) and carrier fluids (nonmagnetic fluids) are used as the main ingredients to make MR fluids.

However, regardless of several benefits as a semi-active actuator, MR fluids have faced a serious problem called sedimentation, when the iron particles settle down to the bottom of the container. The force of gravity causes iron particles to gradually settle to the bottom caused by the noticeable dissimilarity in the density of CIPs (7.5 g/cm^3) and carrier fluids (1 g/cm^3) [8]. Notably, sedimentation influences the effectiveness of MR fluids in terms of their MR effect and longevity. Consequently, frequent disposal of MR fluids is common in the application, while its disposal may contribute to severe environmental problems. To prevent this problem, several researchers have proposed diverse recipes related to material composition modifications [9]. An enhancement was proposed by Zhibin et al. [10] by modifying the carrier fluids in which the molybdenum disulfide created a high zero-field thickness, a small contact angle, and a good wetting impact leading to the antisedimentation within MR fluids like the grease. Cheng et al. [11] coated the surface of iron particles with organic molecules as the additive in their experiment. This increased suspension stability and decreased sedimentation rate without drastically lessening the magnetorheological effect. Another recent study by E.T. Maharani et al. [12] experimented with a sedimentation test of commercial MR fluids (MRF-132DG) by applying several current input magnitudes with different current profiles (sine and square waves) to improve sedimentation stability. The study proved that the current input of 1.5 A, generated from an electromagnetic field of 0.073 T, could prevent the occurrence of sedimentation.

The evaluation of sedimentation stability of MR fluids can be done using several methods. Tensiometric tools, such as Krüss K100, have been developed [13,14] to measure the sedimentation velocity in the stable position. S.R. Gorodkin et al. [15] proposed measuring the sedimentation velocity using the magnetic conductivity of dispersed iron particles in the MR fluids. G.R. Iglesias [16,17] modified S.R. Gorodkin's device to allow a tube filled with MR fluids to be fully scanned using a measuring coil. The volume fraction of iron particles was determined by the inductance (L) of a thin coil surrounding the test tube. Another study by M.T. López-López et al. [18,19] designed a device using two large Helmholtz coils to generate a low-intensity AC magnetic field. The test tube was placed inside a stationary sensing coil at the center of the field, allowing only localized sedimentation to be surveyed. Another study by M. Lita et al. [20] utilized an x-ray transmission with a Dron 3 diffractometer to characterize the sedimentation rate. This device had a stationary probe that measured concentration at a specific location. H. Cheng et al. [21] introduced a method to measure the sedimentation rate by correlating the thermal conductivity of MR fluids with particle concentration. This method used a thermal conductivity tester with a 100 mm long probe. However, each mentioned method somehow still has shortcomings that need to be improved. The most used method to evaluate the sedimentation stability of MR fluids sedimentation is visual assessment. This method has been widely used in many studies [22–26] by monitoring the height of the sedimentation layer.

Another factor to consider in the actuating properties of the semi-active MR actuator is temperature, which varies depending on the environmental and operational conditions of the application systems. The sedimentation test based on different temperatures was performed by a few researchers. A.K. Kariganaur et al. [27] investigated the effect of temperature (30 °C to 100 °C) on the sedimentation stability of six different kinds of MR fluids with different compositions in additives (lithium grease and calcium grease) and carrier fluids (silicone oil and hydraulic oil). They investigated the sedimentation stability under off-state conditions in different temperatures controlled using an incubator. A rheometer was also used with different testing parameters (temperature and magnetic field) to compare the

rheological properties of MR fluids. The study has stated that the settling particle is significantly influenced by temperature. A temperature increase causes a significant decrement in the viscosity and density of the carried fluids, increasing the mismatch density, which causes faster settling of particles. In addition, the combination of silicone oil carrier fluid and lithium base grease additive exhibits superior long-term, particle-retaining capacity at higher temperatures. Another recent study by Y. Rabbani et al. [28] explored sedimentation stability, rheological properties, and the magnetorheological effect of carbonyl iron microparticles (CIMs) suspended in silicone oil across temperatures from 10 to 85 °C using a water bath that had a thermal control. The findings reported that additives could be used to prepare stable and effective MR fluids, which was proved by the sedimentation stability of over 92% at 25 °C. Furthermore, it has been found that the maximum yield stress increases sharply with increasing magnetic field strength or decreasing temperature. In addition, the temperature has a significant impact on the characteristics of MR fluids and thermal conductivity [29]. The causes and recipes to resolve or reduce the particle sedimentation of MR fluids have been well summarized in the previous study by S.B. Choi [9]. So far, many studies on the particle sedimentation of MR fluids have been carried out by reducing the mass density of the magnetic particles through the addition of additives and particle coatings and the use of different particle shapes from spherical ones such as flakes. However, a relationship between the sedimentation rate and temperature variation at various magnetic fields has not been reported yet. Moreover, the field-dependent actuating forces subjected to sedimentation and temperature variation have not been identified either. In the calculation of the actuating force, the principal rheological properties of MR fluids, such as viscosity, storage modulus, and yield stress, are required.

Consequently, the main technical contribution of this work is to experimentally investigate a relationship between the field-dependent actuating force and the particle sedimentation of MR fluids at different temperatures. In order to achieve this goal, a magnetic analysis of a multiguide-arm magnetic device is undertaken using a finite element method magnetics to obtain the predicted generated magnetic flux density, followed by an experimental investigation of the temperature variation with respect to the time. In this study, several current magnitudes from a DC source and controlled temperatures are imposed on MR fluids over a long-term period (168 h). Experimental results include the sedimentation stability by visual observation to obtain the sedimentation rate and the rheological properties of MR fluids such as viscosity, shear stress, and yield stress at different current levels. To verify the actuating performance of the semi-active actuator of MR fluids, mathematical modeling is used to obtain damping force using the results achieved in different testing conditions. It is remarked here that the results presented in this work will be an effective reference for the calculation of the actuating force of MR application systems without and with particle sedimentation at various temperatures and magnetic field intensities over a long operational period.

2. Materials and Methods

2.1. Magnetic Field Analysis

In this work, a single guide arm magnetic analysis was performed at a certain position of a tube filled with MR fluids due to geometric limitations [12,30]. As a result, the magnetic field does not influence the overall MR fluids region. Therefore, this study proposes a multi-guide-arm magnetic device. A 2-D finite element program, Finite Element Method Magnetics (FEMM 4.2), was used to estimate the generated magnetic flux density and magnetic flux lines around the MR fluids on each position of the magnetic guide arm (top, middle, and bottom). This simulation program has been widely used by other researchers [31–34] to obtain magnetic field analysis. The simulation was started by determining the chosen problem. In this work, the MR fluid 132-DG from LORD Corporation was used which has typical properties as shown in Figure 1a and Table 1 [35]. The guide arm was manufactured using steel 45C (Figure 1b), while the magnetic circuit consisted of a copper wire (1 mm diameter) that wound around the steel bobbin with 500 turns.

Then, the current inputs of 1 A and 2 A were applied to the copper wire to generate the magnetic field through the guide arms. The magnetic field analysis was started by making a two-dimensional design with an air boundary made with the chosen materials, as shown in Figure 2. Then, mesh and simulation results were done. The geometric configuration and simulation results are depicted in Figures 2 and 3, respectively. As shown in Figure 3, uniform magnetic flux lines around the MR fluids were seen in each guide arm with a distance of 19 mm of each position (top, middle, bottom). According to the simulation results, the magnetic flux density around the observation region of the middle position was approximately 0.046 T at 1 A and 0.093 T at 2 A. Meanwhile, the observation region of the top and bottom positions had the same value of magnetic flux density which was roughly 0.027 T and 0.054 T at the current inputs of 1 A and 2 A, respectively. The higher magnetic flux density observed in the middle position arose from the reinforcement magnetic field from the top and bottom guide arms [36]. As shown in Figure 3, the magnetic flux lines pass through and reinforce the magnetic flux at the middle guide arm. The magnetic field was also measured with a Tesla meter (FH-54) equipped with a hall probe (HS-TGB5-104010). The measured magnetic field was nearly similar to the simulation results of approximately 0.046 T for a current input of 1 A and approximately 0.1 T for a current input of 2 A.

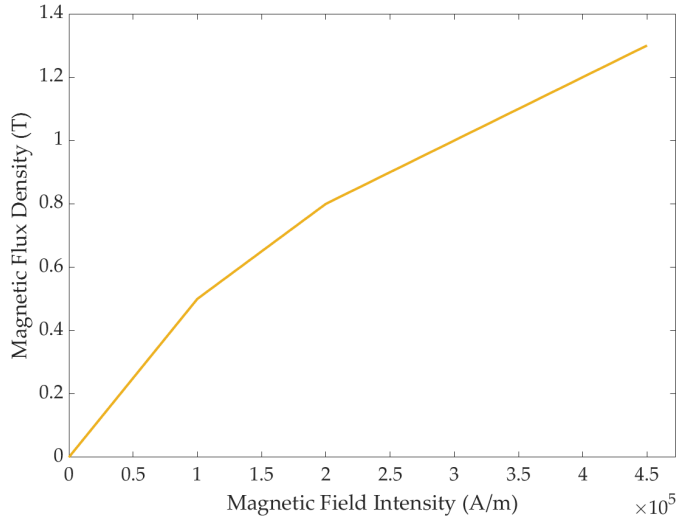

(**a**)

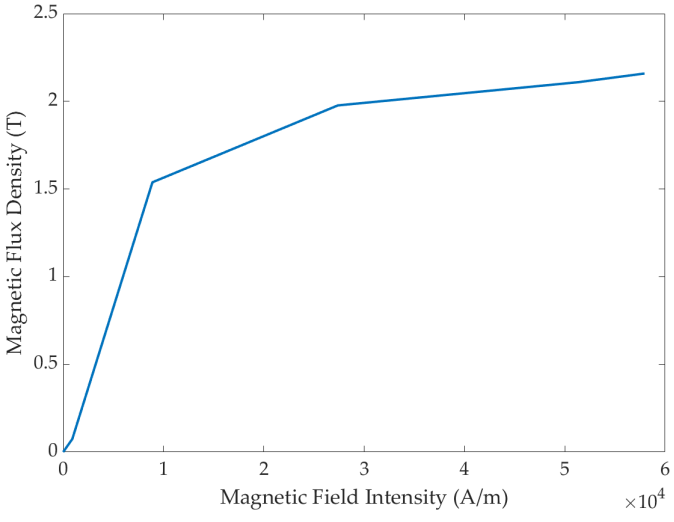

(**b**)

Figure 1. B-H curve (**a**) MR fluid 132-DG (**b**) Steel 45C.

Table 1. Typical properties of MR fluid 132-DG.

Parameters	Value	Unit
Viscosity	0.112	Pa·s
Density	2.95 to 3.15	g/cm^3
Solid Content by Weight	80.90	W%
Flash Point	>150	°C
Temperature	−40 to +130	°C

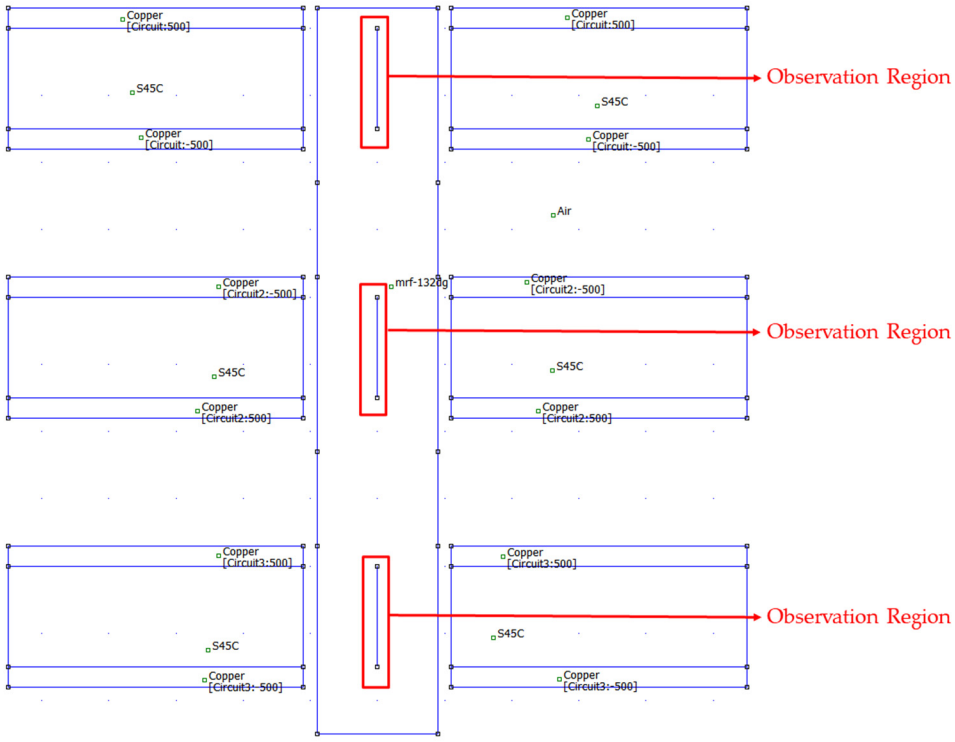

Figure 2. Geometric configuration.

2.2. Experimental Method

The experimental setup of this study was inspired by the previous work by E.T. Maharani et al. [12], with a single guide arm focused only on the top position of a tube filled with MR fluids. However, in this work, a multi-guide-arm magnetic device was subjected to three different positions (top, middle, bottom) of a tube-filled MR fluid to include all the MR fluid regions under the influence of the magnetic field to meet the research objective of this study which investigates several behaviors of MR fluid after long-term operation. Figure 4 shows the working flows of this study. The parameters of our experiment included current input and temperature, which can be seen in Table 2. The overall experimental setup of this study is presented in Figure 5. A DC power supply (GW INSTEK GPS 3303) was used for the source of the current input to the coil that wound to a bobbin. This study used a hot plate (LK Lab Korea H03-04-050) to control the temperature. In addition, a digital thermometer with data logging (SUMMIT TPI 367D) connected with a temperature sensor (TPI STP 150 LB-L) was used to monitor and record the temperature condition of the MR fluids samples.

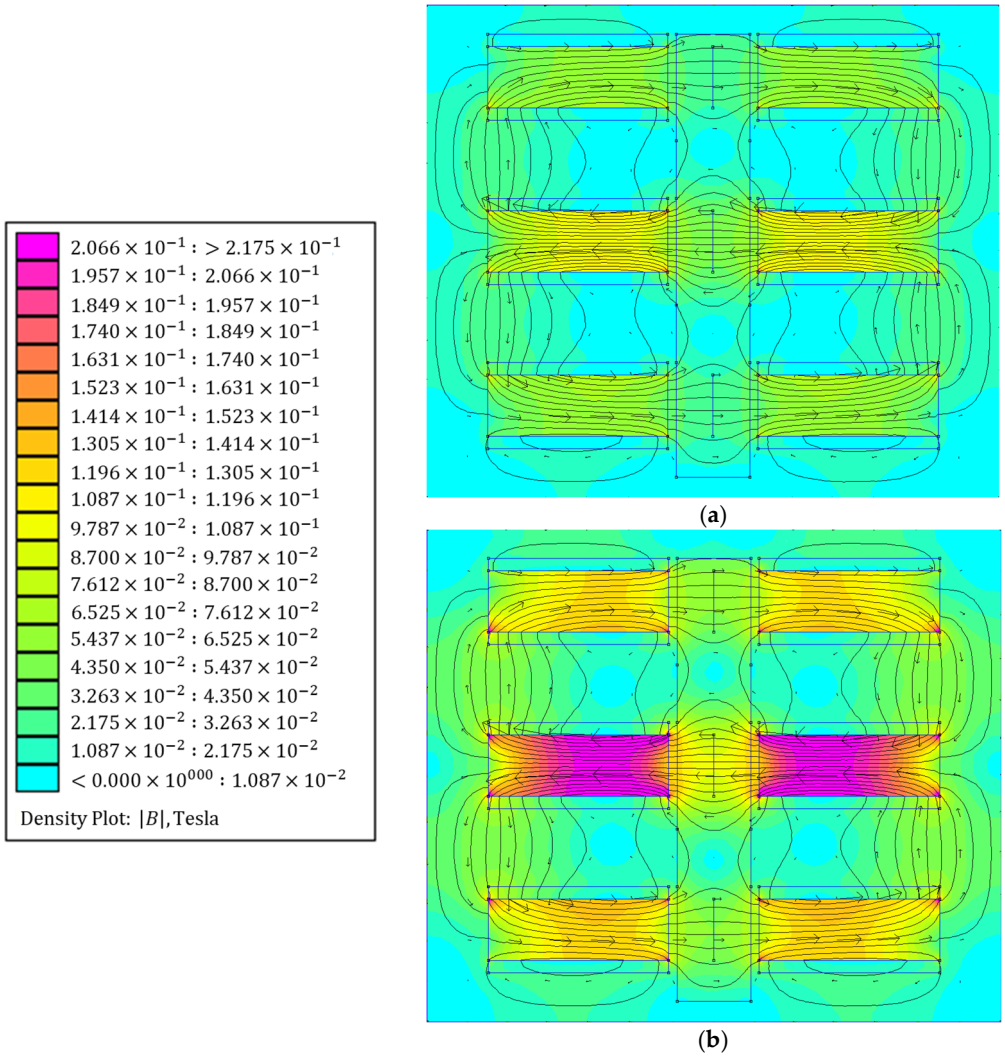

Figure 3. Simulation results of the magnetic field: (**a**) 1 A, (**b**) 2 A.

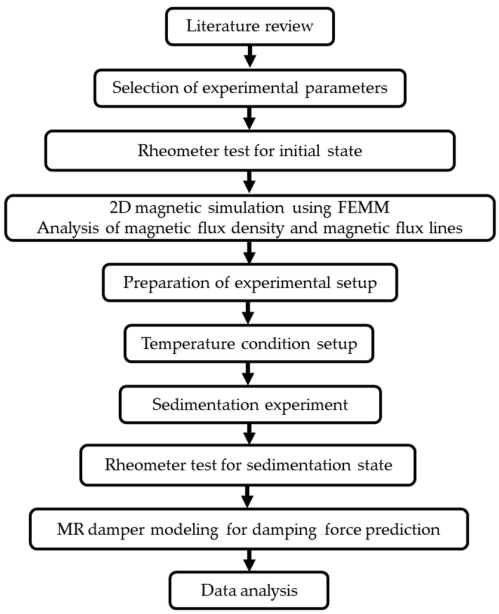

Figure 4. Flow chart of the proposed study.

Table 2. Experimental parameters.

Current Input (A)	Temperature (°C)
0	
1	25
2	
0	
1	50
2	
0	
1	70
2	

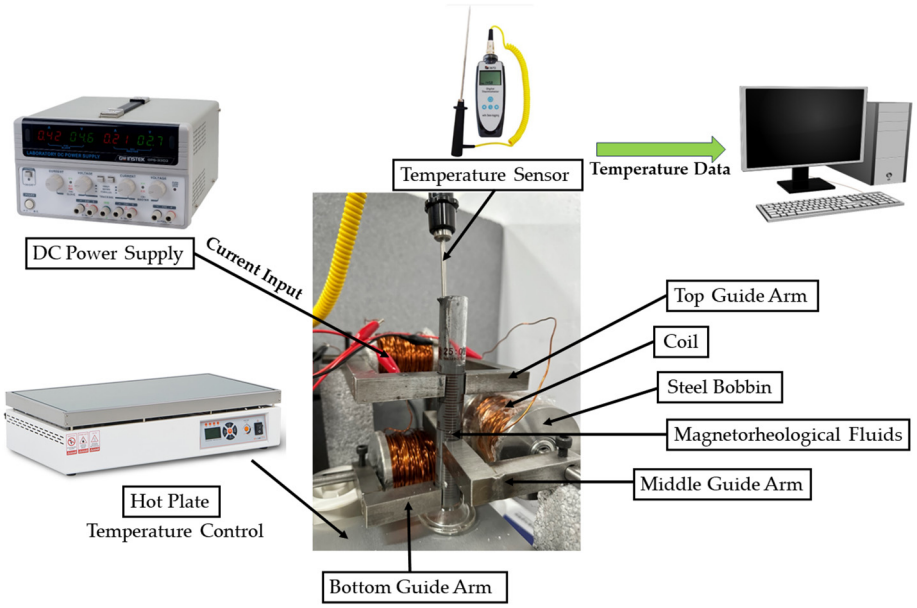

Figure 5. Experimental setup for temperature control and input current supply.

Before the temperature measurement, the tube was placed on the hot plate, and then the measurement was performed. Therefore, the temperature point at 0 s is the initial temperature of the tube on the hot plate. Before filling the tube with MR fluids, we ensured the temperature inside the tube reached the approximate chosen temperatures (25 °C, 50 °C, 70 °C) and was in a stable condition, as shown in Figure 6. In addition, to prevent any leftover sedimentation, we shook the MR fluids with our hands for around fifteen minutes. After the temperature was stable, the MR fluid was poured into the measuring tube until reaching 100 mm to start the experiment.

Many studies have revealed that the most common way to assess the sedimentation of MR fluids is by visually observing the sedimentation layer [25,37,38]. The height measurement of the sedimentation layer was performed after the surface of carrier fluids was seen. The measured height then could be used for the calculation of the sedimentation rate as given in Equation (1). The experiment was performed in a week (168 h) with observations being made every 24 h. Next, for accurate and precise results, the height of the sedimentation layer was measured using a digital caliper.

$$Sedimentation\ Rate\ (\%) = \frac{Height\ of\ sedimentation\ layer}{Total\ height\ of\ MR\ fluids} \times 100\% \quad (1)$$

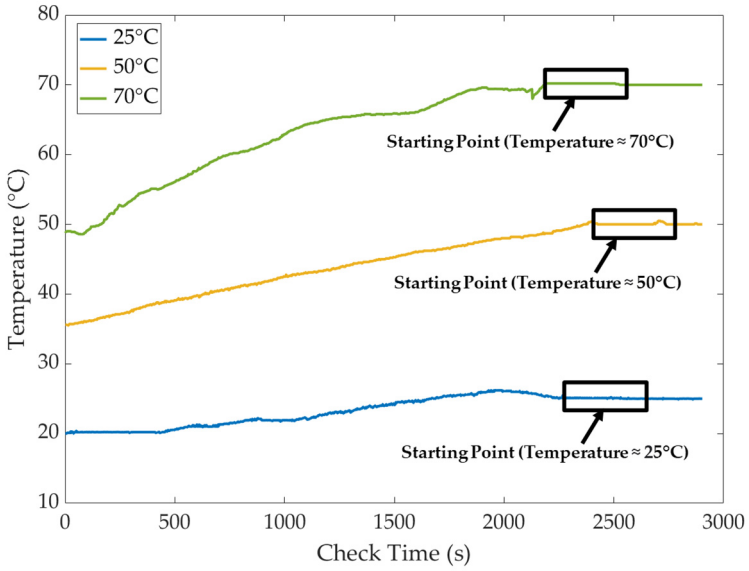

Figure 6. Temperature conditions of sedimentation experiment.

The rheological properties before and after the sedimentation experiment of MR fluid samples were also tested and discussed in this study. A rotational parallel-plate rheometer (MCR302, Anton-Paar, Graz, Austria) that is shown in Figure 7 was used as the testing instrument to obtain the rheological properties of MR fluids. The instrument was connected to a magnetorheological device (MRD 170/1T) equipped with a Tesla meter (FH-54) and a hall probe (HS-TGB5-104010), which can be used to control the current input and generate the magnetic field up to 0.8 T perpendicular to the MR fluids sample. The rheometer is also equipped with the temperature control unit (JULABO 600F) comprising a circulator head and a cooling unit, alongside an electronic proportional temperature controller for regulating the heat supplied to the liquid. This system is to heat or chill the bath tank's liquid. By using this instrument, the temperature-controlled plate can be maintained for the testing conditions, which are 25 °C, 50 °C, and 70 °C, respectively. In addition, the current input of 0 A, 1 A, and 2 A were also applied with the shear rates of 0.01 to 1000 s^{-1}.

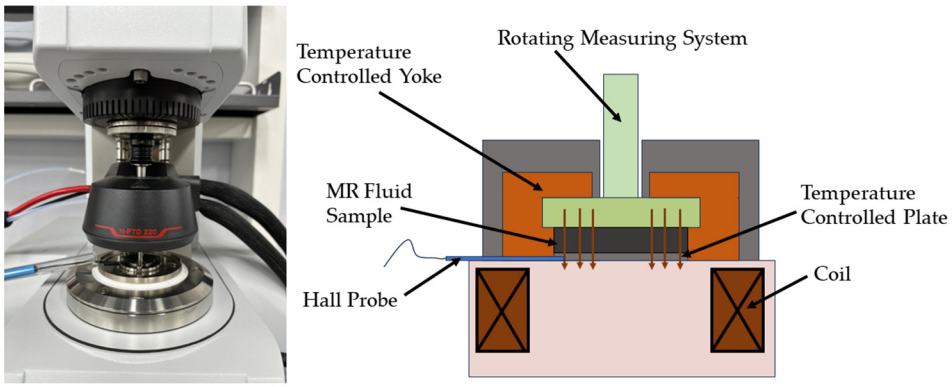

Figure 7. Rheometer configuration.

3. Results and Discussion

3.1. Sedimentation

In this section, the effect of temperature and current inputs on sedimentation stability will be discussed. The sedimentation was evaluated over a total time of 168 h (7 days), with the measurement every 24 h. The experiment was performed under different controlled temperatures (25 °C, 50 °C, 70 °C) at different current inputs of 0 A, 1 A, and 2 A. The sedimentation rate results under various temperatures at current inputs of 0 A, 1 A, and

2 A, are shown in Figure 8. The average sedimentation rate listed in Table 3 is defined as the mean or typical rate of the settling particles of MR fluids over the total experiment period. These values can be obtained by calculating the total value of the sedimentation rate each day and then dividing by the overall duration (7 days). It has been identified that the average sedimentation rate becomes faster with a higher temperature and lower current input conditions. The lower sedimentation rate was owned by the sample under the temperature of 25 °C at 2 A. According to the observation results, the settling particles started after 144 h with a sedimentation rate of 99.8%; then, it ended the next day with a value of 99.4%. In this case, even though the sedimentation happened faster under the higher influence of high temperature, the current inputs played a significant role in slowing the sedimentation process. The higher current input generates a higher magnetic field, which could strengthen the chain-like structure interaction of the carbonyl iron particles [12]. The sedimentation was unstable and started faster sedimentation at a temperature of 50 °C. At the off-state condition, the sedimentation began after 48 h with a sedimentation rate of 99.6% and ended at 96.7%. Meanwhile, the highest sedimentation rate was observed under the temperature of 70 °C at the off-state condition (0 A). It started at 98.8% after 24 h and dropped to a low of 95.5% after 168 h. The study that was done by A. K. Kariganaur [27], and Y. Rabbani [28] observed sedimentation stability under the off-state condition, which also showed that the higher temperature influences sedimentation instability. The possible reasons for the faster sedimentation at higher temperatures were the viscosity and the changes of magnetic particles, which could influence their magnetic properties, to be discussed in Section 3.2.

3.2. Rheological Properties

Rheological properties are the features of MR fluids that represent their characteristics under exposure to the magnetic field. In this study, the results include the rheological properties of the MR fluids before and after the sedimentation experiment. Before conducting the rheometer test, both samples of MR fluids before and after the sedimentation experiment were shaken to obtain suitable samples for testing. The obtained rheological properties (viscosity, shear stress, yield stress) before and after the sedimentation experiment are measured, respectively. To increase readability, the results before the sedimentation experiment are shown as the initial state, while the results after the sedimentation experiment are shown as the sedimentation state. Figure 9 shows the relationship between viscosity and shear rate before and after the sedimentation experiment under the different temperatures (25 °C, 50 °C, 70 °C) and current inputs (0 A, 1 A, 2 A). In both off-state and on-state testing parameters, the MR fluids' viscosity decreased as the shear rate increased. This is known as the shear thinning behavior [39]. Furthermore, the increase of the current input affected the generated magnetic field, which increased the MR fluids' viscosity. The greater the magnetic field applied to the MR fluids resulted the greater the induction of the magnetic particles. This causes a higher attractive force between the magnetic particles. During this condition, the magnetic particles cannot move freely, creating a chain-like structure that can increase the viscosity [40–42]. Meanwhile, as the temperature rose, the viscosity declined, as also reported in a previous study [28]. It was discovered that the viscosity of MR fluid was influenced by the viscosity of the carrier fluid. As the temperature increased, the viscosity of the carrier fluid decreased. Furthermore, the carrier fluid with higher viscosity showed a greater sensitivity to temperature changes [43]. The decreased value in viscosity may cause the reduction of the resistance to particle movement. Then, the particle settlement will be faster because the fluid offers less resistance to the movement of iron particles through it. This is one of the factors that influence the instability of sedimentation. The viscosity after the sedimentation experiment under both off-state and on-state conditions became lower than before the sedimentation experiment. This is likely because of the significant molecular spacing. When the MR fluids were subjected to the controlled temperature for a long time, it disrupted the arrangement of iron particles within the fluids, causing an increase in kinetic energy between them. This resulted in greater spacing between iron

particles, reducing internal friction and consequently lowering the viscosity of the MR fluids [44].

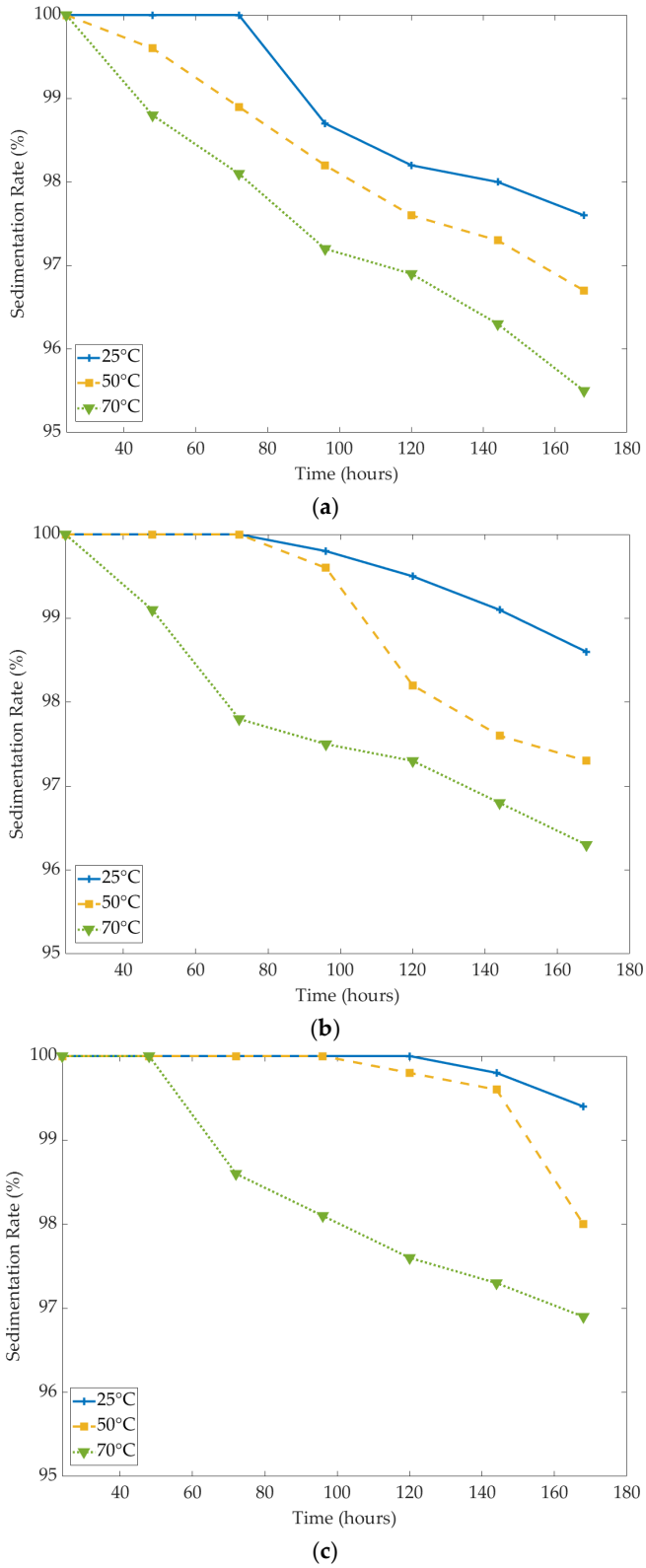

Figure 8. Sedimentation rate under various temperatures of 25 °C, 50 °C, and 70 °C at current inputs of (**a**) 0 A, (**b**) 1 A, (**c**) 2 A.

Table 3. The average sedimentation rate.

Temperature T (°C)	Current Input I (A)	Average Sedimentation Rate (%)
25	0	98.93
	1	99.57
	2	99.89
50	0	98.33
	1	98.81
	2	99.63
70	0	97.54
	1	98.17
	2	98.36

On the other hand, the shear stress plays a crucial role in determining the performance of MR fluids. A higher shear stress value implies that the MR fluids require a lower magnetic field strength to control MR characteristics. A lower magnetic field for MR application may decrease the required electrical energy. Figure 10 depicts the results of the relationship between shear stress and shear rate under the different temperatures (25 °C, 50 °C, 70 °C) at various current inputs (0 A, 1 A, 2 A). It can be seen in Figure 10a that under off-state conditions, as the shear rate increases, the shear stress rises almost linearly, which is known as Newtonian fluids [45]. Meanwhile, under the on-state condition (Figure 10b,c), the shear stress showed a higher value than the off-state condition. When the higher current input was applied, the generated magnetic field increased. This is attributed to the formation of chain-like structures exhibiting Bingham plastic behavior [46]. Regarding the effect of the temperature, the shear stress of the MR fluids decreased as the temperature increased. As expected, it is obvious that the MR fluids after the sedimentation experiment had a lower shear stress compared to the shear stress values before the sedimentation experiment. This was because the viscosity of the MR fluids declined under the long-term influence of high temperatures that affected the shear stress [47]. Furthermore, the changes in the hydrodynamic force following the Navier–Stokes law might have contributed to the decrement of shear stress [29].

3.3. Actuating Properties

It is well known that the field-dependent yield stress directly relates to the actuating force of the semi-active MR actuator. Yield stress represents the threshold that must be exceeded to initiate flow in MR fluids. It is the most important property of MR fluids that determines their transition from a solid-like to a liquid-like state [48]. Even though the maximum yield stress could be achieved at the higher current input, the yield stress certainly declined as the higher temperature following the after-sedimentation experiment had lower yield stress values. When the yield stress has a low value, MR fluids start flowing easily, which reduces their controllable and tunable ability. Consequently, it would degrade the performance of the MR fluid applications such as MR damper, MR brake, and MR clutch, which require a high and tunable yield stress [49,50]. An MR damper was selected as a target actuator [51] for further analysis of the actuating performance of the MR fluids on initial and sedimentation states. The configuration of the MR damper includes a piston, cylinder, and gas chamber, which can be seen in Figure 11. Mathematical modeling was done using the parameters listed in Table 4. There are upper and lower chambers that are divided by the piston and the MR fluids flow inside the chamber through the annular duct. The cylinder is filled with MR fluids, while the gas chamber is filled with nitrogen gas. The magnetic circuit at the top and bottom of the annular duct controls the yield stress value of MR fluids.

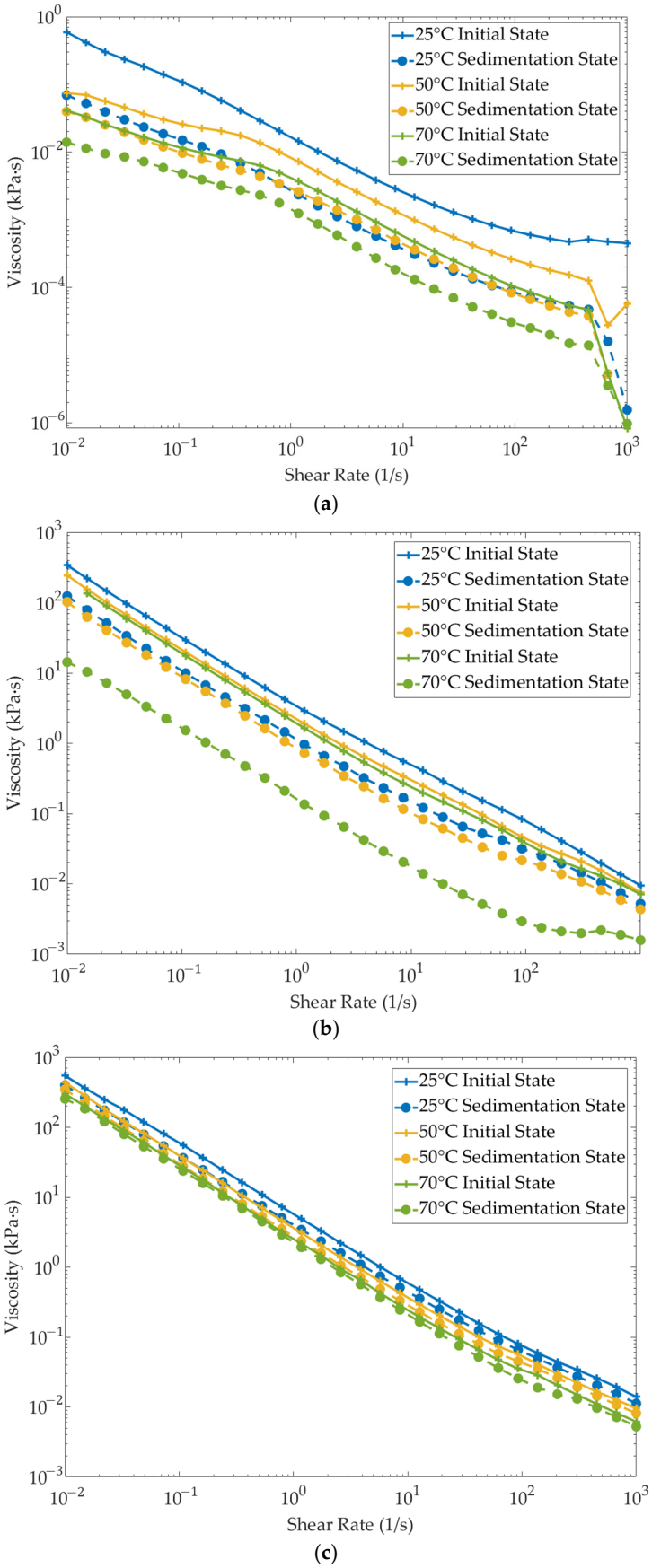

Figure 9. The viscosity of MR fluids for initial and sedimentation states under the controlled temperatures of 25 °C, 50 °C, and 70 °C at current inputs of (**a**) 0 A, (**b**) 1 A, (**c**) 2 A.

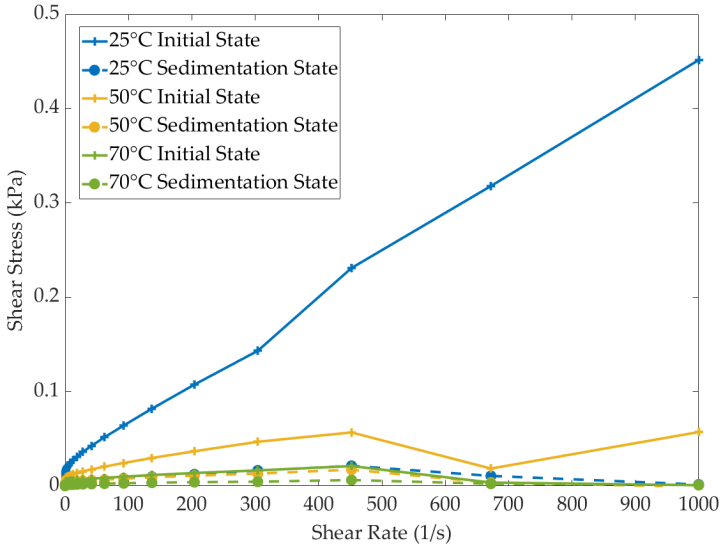

(**a**)

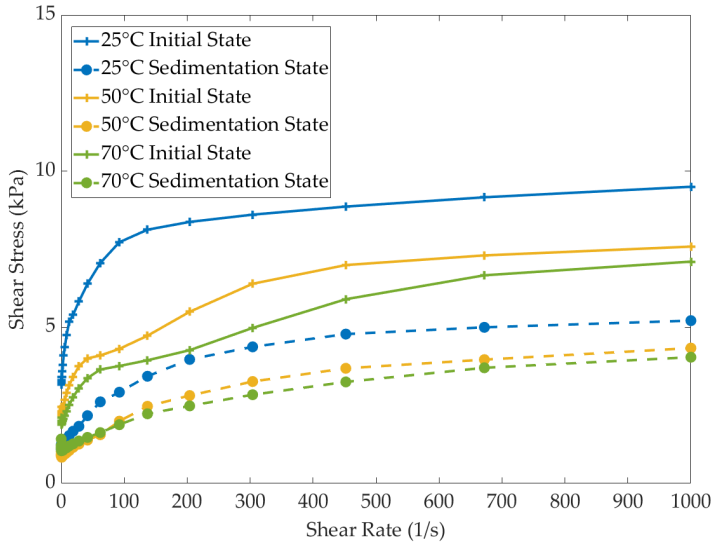

(**b**)

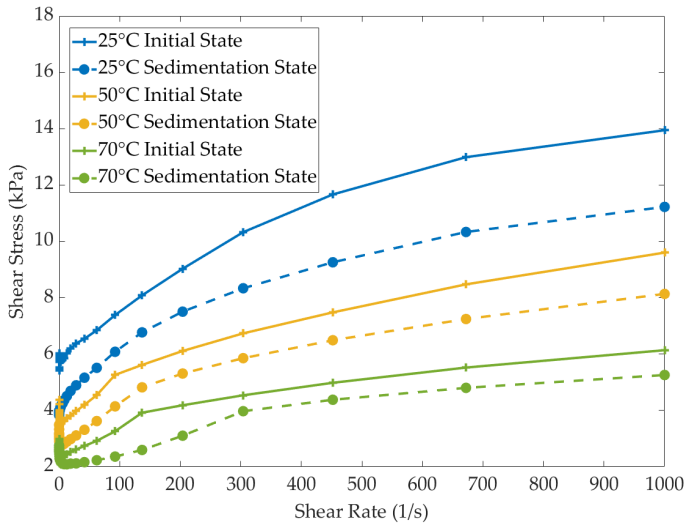

(**c**)

Figure 10. Shear stress of MR fluids for initial and sedimentation states under the controlled temperatures of 25 °C, 50 °C, and 70 °C at current inputs of (**a**) 0 A, (**b**) 1 A, (**c**) 2 A.

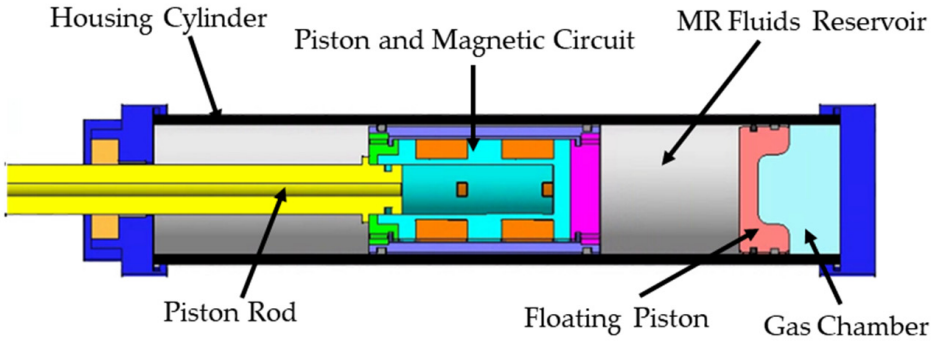

Figure 11. Section view of MR damper.

Table 4. Parameters of MR damper.

Parameter	Description	Value	Unit
L_d	Effective pole length	50	mm
L	Length of the annular duct	150	mm
r_p	Radius of piston	28.2	mm
r_s	Radius of piston shaft	20.34	mm
b	Duct width	174	mm
c	Coefficient of the flow velocity	2.07	
h	Gap of annular duct	1	mm

The damping force (F_d) of MR damper can be presented as given in Equation (2) [52]. Without the magnetic influence (off-state condition), the damping force is generated from the fluid viscous resistance of the MR damper. Meanwhile, under the magnetic field influence (on-state condition), the damping force has an additional value because of the existing yield stress. In other words, the generated damping force can be tuned based on the intensity of the magnetic field. The gas force (F_{gas}) due to the accumulator and friction forces $\left(F_{friction}\right)$ within the MR damper can be obtained through experiments. However, it is usually omitted in formal calculations for simplification purposes.

$$F_d = c_e\,\dot{x}_p + F_{MR} + F_{gas} + F_{friction} \tag{2}$$

In the above, the effective damping coefficient can be obtained by

$$c_e = \left(A_p - A_s\right)^2 R_e \tag{3}$$

where $\dot{x}_p$ is the velocity of the piston, A_p is the area of the piston, A_s is the area of the piston shaft, while fluid resistance (R_e) can be defined as

$$R_e = \frac{12\eta L}{bh^3} \tag{4}$$

where η is the viscosity of MR fluids, L is the length of the annular duct, b is duct width, and h is the gap of the annular duct. Meanwhile, F_{MR} can be obtained using the Equation (3) as written below

$$F_{MR} = c\frac{L_d}{h}(A_p - A_s)\tau_y sgn(\dot{x}_p) \tag{5}$$

where c is the flow function coefficient, L_d is the effective pole length, h is the length of the orifice, $\dot{x}_p$ is the velocity of piston, $sgn(\cdot)$ is a signum function, and τ_y is the yield stress at a certain magnetic flux density. The yield stress value was obtained by extrapolating the shear stress curve when the shear rate is zero [53,54], or by describing the shear stress according to a rheological model obtained from the rheometer test [55]. After all,

the most widely used model is the Bingham-plastic model for viscoplastic flow. Based on the Bingham-plastic model, the shear stress is expressed as

$$\tau = \tau_y + \eta_p \dot{\gamma}, \quad \dot{\gamma} > 1 \tag{6}$$

where τ is shear stress, τ_y is yield stress under magnetic field influence, η_p is viscosity defined as the gradient of the shear stress versus shear rate graph at elevated shear rates, and $\dot{\gamma}$ is shear rate [28,56]. The obtained yield stress value of the initial and sedimentation states of MR fluids are depicted in Figure 12 and listed in Tables 5 and 6. It shows that current input and temperature have a significant role in obtaining the maximum yield stress. A similar finding was reported by Y. Rabbani et al., which showed a decrement in yield stress value at a higher temperature [28]. Furthermore, the yield stress of the initial state showed a higher value than the sedimentation state. Based on Figure 11, the yield stress showed nearly zero for all temperature conditions under the off-state condition (0 A) as the Bingham model, where the yield stress approaches zero as the magnetic field approaches zero. Meanwhile, at 70 °C, the yield stress under the on-state condition (2 A) declined from 2.747 kPa (initial state) to 2.352 kPa (sedimentation state).

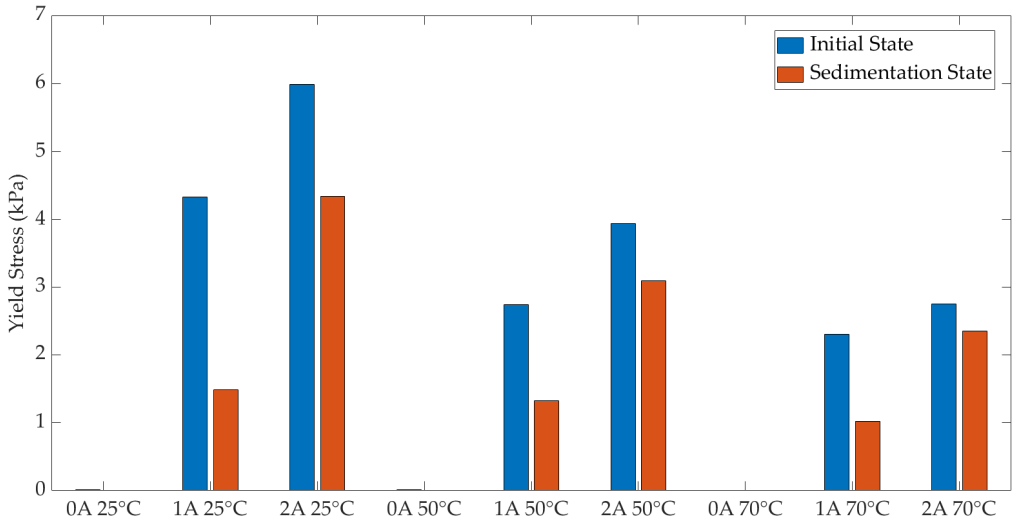

Figure 12. Yield stress under different controlled temperatures of 25, 50, and 70 °C at current input of 0 A, 1 A, 2 A for initiate state and sedimentation state.

Table 5. The obtained viscosity, shear stress, and yield stress of the initial state.

Temperature T (°C)	Current Input I (A)	Viscosity η_p (kPa·s)	Shear Stress τ (kPa)	Yield Stress τ_y (kPa)
25	0	0.593	0.00593	0.016
	1	341	3.402	4.332
	2	547	5.467	5.988
50	0	0.075	0.000746	0.0095
	1	245	2.445	2.745
	2	438	4.374	3.950
70	0	0.041	0.000410	0.005
	1	211	2.109	2.303
	2	300	2.998	2.747

Table 6. The obtained viscosity, shear stress, and yield stress of the sedimentation state.

Temperature T (°C)	Current Input I (A)	Viscosity η_p (kPa·s)	Shear Stress τ (kPa)	Yield Stress τ_y (kPa)
25	0	0.069	0.000694	0.004
	1	123.7	1.237	1.486
	2	399.05	3.9893	4.349
50	0	0.0397	0.000397	0.0038
	1	102.34	1.024	1.321
	2	349.5	3.493	3.094
70	0	0.041	0.00014	0.0015
	1	14.24	1.421	1.021
	2	255.39	2.553	2.352

Using Equation (2), the damping force was calculated. Figure 13 shows the dynamic range of the MR damper. The dynamic range of the MR damper plays a significant role in determining the extent to which MR fluids' rheological properties can be adjusted and controlled, allowing it to transition from a free-flowing liquid to a semi-solid state that enables precise control over damping performance. It is defined using the F-V plot as the area between the MR fluids' maximum yield stress when subjected to the strongest magnetic field (2 A) and their minimum yield stress when there is no magnetic influence (0 A). A higher dynamic range indicates greater control over the MR fluids' behavior, allowing a wide tunable range for MR applications. It is clearly seen that the damping force of the sedimentation state showed a degradation performance compared to the initial state under a higher temperature, indicated by the lower tunable range of the field-induced damping force. The widest tunable range was shown on the results of the initial state under the temperature of 25 °C. Meanwhile, the lowest tunable range of damping force was shown on the sedimentation state under the temperature of 70 °C. Furthermore, it is known that to achieve both optimal ride comfort and road holding, a high damping coefficient is needed at low-stroke velocities, whereas a low damping coefficient is needed at high-stroke velocities. A slope breaking point can be determined to identify the changes in damping characteristics [57]. In this study, the lowest velocity of 0.005 m/s was chosen to determine this point. Based on the results, the slope breaking point was 751.16 N for the initial state under a temperature of 25 °C at a current input of 2 A. However, the slope breaking point decreased to 547.83 N for the sedimentation state under a temperature of 25 °C at a current input of 2 A. The reduction in the slope breaking point was also seen in the other experimental temperatures of 50 °C and 70 °C at a current input of 2 A after sedimentation, as shown in Table 7. Overall, it can be noted that the sedimentation of MR fluids after being subjected to the long-term influence of temperature and magnetic field degraded the actuating properties of MR fluids. The possible reason is because of the declining value of their rheological properties (viscosity, shear stress, and yield stress) that were discussed in previous Section 3.2. A previous experimental study using MR damper by N.L. Wilson et al. [58] also reported a similar tendency regarding the temperature effect on the damping performance up to 37% at the current input of 2.5 A under the temperature of 100 °C without considering the sedimentation.

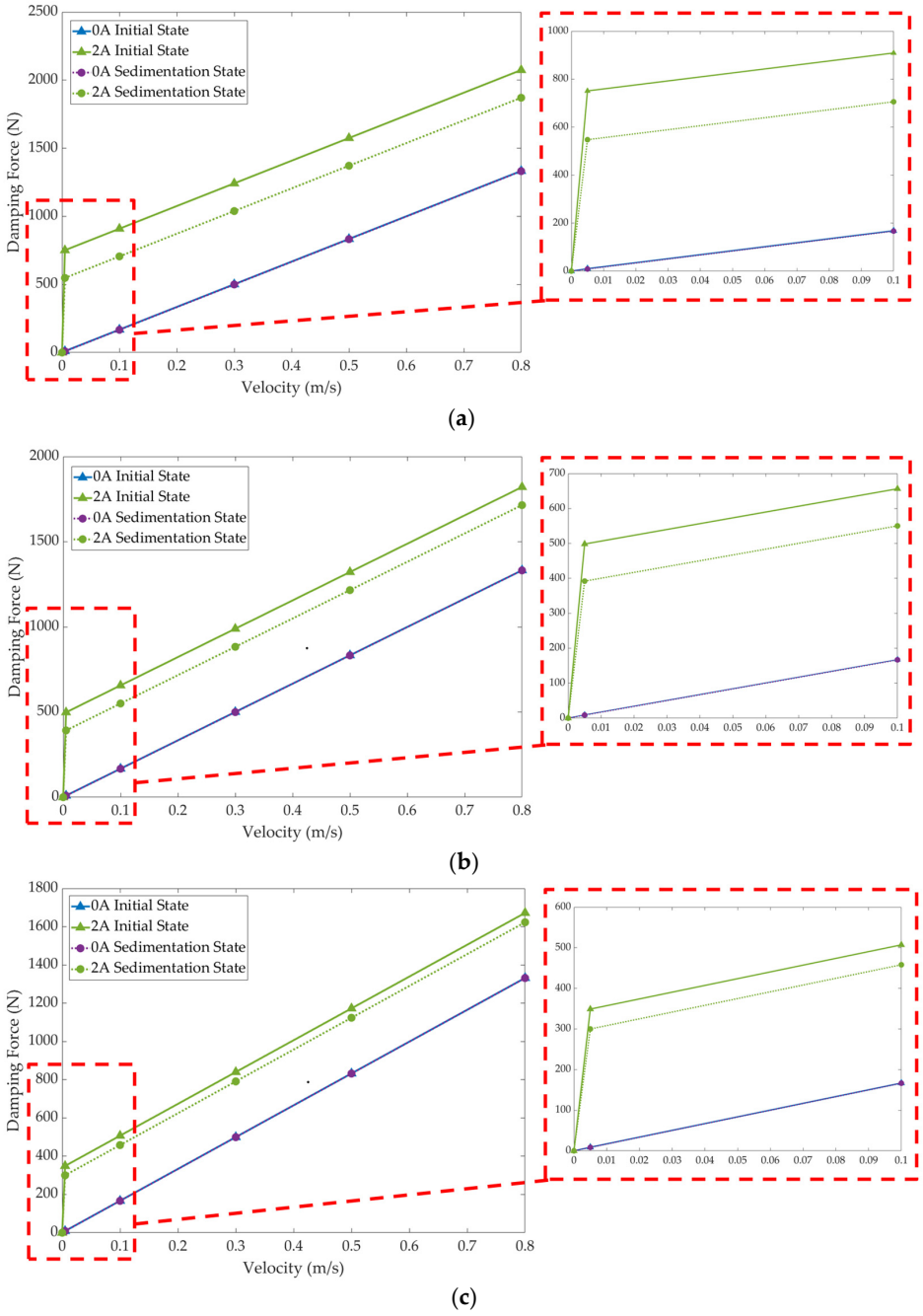

Figure 13. MR damper dynamic range at temperatures of (**a**) 25 °C, (**b**) 50 °C, (**c**) 70 °C.

Table 7. Slope breaking point.

Current Input (A)	Temperature (°C)	Condition	Damping Force (N)
2	25	Initial State	751.16
		Sedimentation State	547.83
	50	Initial State	498.34
		Sedimentation State	392.15
	70	Initial State	349.09
		Sedimentation State	300.09

4. Conclusions

This work conducted an experimental study using a multi-guide-arm magnetic device that generated a uniform magnetic field throughout the MR fluid. This method was used to

observe the sedimentation stability of MR fluids under the different controlled temperatures (25, 50, 70 °C) for a long-term period with the applied current inputs of 0, 1, 2 A. The findings revealed that experimental parameters of lower temperature (25 °C) and higher current input (2 A) resulted in the highest sedimentation rate, indicating the slowest sedimentation, with an average rate of 99.89%. Meanwhile, the lowest sedimentation rate achieved was 97.54% under off-state conditions (0 A) at a temperature of 70 °C. The decrease in viscosity after the influence of high temperature is believed to be the cause of sedimentation increment of MR fluids. This study also investigated the rheological properties (viscosity, shear stress, yield stress) of the MR fluids before and after the sedimentation experiment. When the temperature was increased, the measured rheological properties decreased drastically for the MR fluid samples before the sedimentation experiment. Additionally, according to the results, the rheological properties experienced a significant decline after the sedimentation experiment following the increase in temperature. Nevertheless, the maximum yield stress could be achieved after the application of the highest current input. In order to validate the actuating performance of the MR fluids, the damping force of an MR damper was calculated. The results showed that the actuating properties of MR fluids declined significantly after the sedimentation experiment, which related to the long-term effects of temperature and magnetic fields. This is most likely caused by the degradation of the rheological properties (viscosity, shear stress, yield stress) of MR fluids.

In conclusion, it was proven that even though the current input (magnetic field) could slow the sedimentation of MR fluids, the long-term high temperatures undoubtedly led to the fast sedimentation and the degradation of their rheological properties of MR fluids. It is finally noted that the sedimentation problem of magnetic particles should be resolved by considering both the temperature increment due to a long-term operation as well as the magnitude of the flux density to achieve the required actuating force of the semi-active actuator, magnetorheological fluids.

Author Contributions: Conceptualization, E.T.M., D.-H.L., J.-S.O. and S.-B.C.; methodology, D.-H.L., E.T.M., J.-S.O. and S.-B.C.; software, D.-H.L., E.T.M. and Y.-J.K.; validation, E.T.M., D.-H.L., Y.-J.K., J.-S.O. and S.-B.C.; formal analysis, E.T.M., D.-H.L., Y.-J.K., J.-S.O. and S.-B.C.; investigation, D.-H.L. and E.T.M.; resources, E.T.M., D.-H.L., Y.-J.K., J.-S.O. and S.-B.C.; data curation, E.T.M., D.-H.L., Y.-J.K. and J.-S.O.; writing—original draft preparation, E.T.M.; writing—review and editing, E.T.M., J.-S.O. and S.-B.C.; visualization, E.T.M., D.-H.L. and Y.-J.K.; supervision, J.-S.O. and S.-B.C.; project administration, J.-S.O.; funding acquisition, J.-S.O. and S.-B.C. All authors have read and agreed to the published version of the manuscript.

Funding: This research was partially supported by the "Regional Innovation Strategy (RIS)" through the National Research Foundation of Korea (NRF) funded by the Ministry of Education (MOE) (2021RIS-004) and the Korea Government (MSIT) (No. 2022R1F1A1074691).

Data Availability Statement: The data used to support the findings of this study are included within the article.

Conflicts of Interest: The authors declare no conflicts of interest.

References

1. De Vicente, J.; Klingenberg, D.J.; Hidalgo-Alvarez, R. Magnetorheological Fluids: A Review. *Soft Matter* **2011**, *7*, 3701–3710. [CrossRef]
2. Hu, G.; Ying, S.; Qi, H.; Yu, L.; Li, G. Design, analysis and optimization of a hybrid fluid flow magnetorheological damper based on multiphysics coupling model. *Mech. Syst. Signal Process.* **2023**, *205*, 110877. [CrossRef]
3. Kluszczyński, K.; Pilch, Z. The choice of the optimal number of discs in an mr clutch from the viewpoint of different criteria and constraints. *Energies* **2021**, *14*, 6888. [CrossRef]
4. Eem, S.-H.; Koo, J.-H.; Jung, H.-J. Feasibility study of an adaptive mount system based on magnetorheological elastomer using real-time hybrid simulation. *J. Intell. Mater. Syst. Struct.* **2018**, *30*, 701–707. [CrossRef]
5. Ubaidillah, U.; Imaduddin, F.; Nizam, M.; Mazlan, S.A. Response of A Magnetorheological Brake under Inertial Loads. *Int. J. Electr. Eng. Inform.* **2015**, *7*, 308–322.
6. Kemerli, M.; Şahin, Ö.; Yazıcı, İ.; Çağlar, N.; Engin, T. Comparison of discrete-time sliding mode control algorithms for seismic control of buildings with magnetorheological fluid dampers. *J. Vib. Control* **2022**, *29*, 1752–1765. [CrossRef]

7. Ganapathy Srinivasan, R.; Shanmugan, S.; Palani, S. Application of magnetorheological fluid in machining process. *Int. J. Control Theory Appl.* **2016**, *9*, 3705–3712.
8. Prajapati, H.; Shahanand, J.; Nimkar, H.; Lakdawala, A. Methods for sedimentation study of magnetorheological fluids. *Mater. Today Proc.* **2020**, *28*, 40–44. [CrossRef]
9. Choi, S.-B. Sedimentation Stability of Magnetorheological Fluids: The State of the Art and Challenging Issues. *Micromachines* **2022**, *13*, 1904. [CrossRef]
10. Zhibin, S.; Yiping, L.; Ying, W.; Jiao, L.; Dongsheng, J. Study on sedimentation stability of magnetorheological fluids based on different lubricant formulations. *Mater. Res. Express* **2020**, *7*, 085702. [CrossRef]
11. Cheng, H.; Wang, M.; Liu, C.; Wereley, N.M. Improving sedimentation stability of magnetorheological fluids using an organic molecular particle coating. *Smart Mater. Struct.* **2018**, *27*, 075030. [CrossRef]
12. Maharani, E.T.; Seo, M.-W.; Sohn, J.W.; Oh, J.-S.; Choi, S.-B. The Influence of Current Magnitudes and Profiles on the Sedimentation of Magnetorheological Fluids: An Experimental Work. *Magnetochemistry* **2024**, *10*, 18. [CrossRef]
13. Cvek, M.; Mrlik, M.; Ilcikova, M.; Plachy, T.; Sedlacik, M.; Mosnacek, J.; Pavlinek, V. A facile controllable coating of carbonyl iron particles with poly(glycidyl methacrylate): A tool for adjusting MR response and stability properties. *J. Mater. Chem. C* **2015**, *3*, 4646–4656. [CrossRef]
14. Sedlacik, M.; Pavlinek, V. A tensiometric study of magnetorheological suspensions' stability. *RSC Adv.* **2014**, *4*, 58377–58385. [CrossRef]
15. Gorodkin, S.R.; Kordonski, W.I.; Medvedeva, E.V.; Novikova, Z.A.; Shorey, A.B.; Jacobs, S.D. A method and device for measurement of a sedimentation constant of magnetorheological fluids. *Rev. Sci. Instrum.* **2000**, *71*, 2476–2480. [CrossRef]
16. Iglesias, G.R.; Ruiz-Morón, L.F.; Monesma, J.I.; Durán, J.D.G.; Delgado, A.V. An experimental method for the measurement of the stability of concentrated magnetic fluids. *J. Colloid Interface Sci.* **2007**, *311*, 475–480. [CrossRef] [PubMed]
17. Iglesias, G.R.; López-López, M.T.; Delgado, A.V.; Durán, J.D.G. Description and performance of a fully automatic device for the study of the sedimentation of magnetic suspensions. *Rev. Sci. Instrum.* **2011**, *82*, 073906. [CrossRef] [PubMed]
18. López-López, M.T.; Zugaldía, A.; González-Caballero, F.; Durán, J.D.G. Sedimentation and redispersion phenomena in iron-based magnetorheological fluids. *J. Rheol.* **2006**, *50*, 543–560. [CrossRef]
19. López-López, M.T.; de Vicente, J.; Bossis, G.; González-Caballero, F.; Durán, J.D.G. Preparation of stable magnetorheological fluids based on extremely bimodal iron–magnetite suspensions. *J. Mater. Res.* **2005**, *20*, 874–881. [CrossRef]
20. Lita, M.; Han, A.; Susan-Resiga, D. Characterization of sedimentation and high magnetic field flow behavior of some magnetorheological fluids. *J. Phys. Conf. Ser.* **2009**, *149*, 012071. [CrossRef]
21. Cheng, H.; Zhang, X.; Liu, G.; Ma, W.; Wereley, N.M. Measuring the sedimentation rate in a magnetorheological fluid column via thermal conductivity monitoring. *Smart Mater. Struct.* **2016**, *25*, 055007. [CrossRef]
22. Wang, G.; Ma, Y.; Tong, Y.; Dong, X. Development of manganese ferrite/graphene oxide nanocomposites for magnetorheological fluid with enhanced sedimentation stability. *J. Ind. Eng. Chem.* **2017**, *48*, 142–150. [CrossRef]
23. Zhu, W.; Dong, X.; Huang, H.; Qi, M. Iron nanoparticles-based magnetorheological fluids: A balance between MR effect and sedimentation stability. *J. Magn. Magn. Mater.* **2019**, *491*, 165556. [CrossRef]
24. Aruna, M.N.; Rahman, M.R.; Joladarashi, S.; Kumar, H. Investigation of sedimentation, rheological, and damping force characteristics of carbonyl iron magnetorheological fluid with/without additives. *J. Braz. Soc. Mech. Sci. Eng.* **2020**, *42*, 228. [CrossRef]
25. Aruna, M.N.; Rahman, M.R.; Joladarashi, S.; Kumar, H.; Devadas Bhat, P. Influence of different fumed silica as thixotropic additive on carbonyl particles magnetorheological fluids for sedimentation effects. *J. Magn. Magn. Mater.* **2021**, *529*, 167910. [CrossRef]
26. Leong, S.A.N.; Mazlan, S.A.; Samin, P.M.; Idris, A.; Ubaidillah. Performance of bidisperse magnetorheological fluids utilizing superparamagnetic maghemite nanoparticles. *AIP Conf. Proc.* **2016**, *1710*, 030050.
27. Kumar Kariganaur, A.; Kumar, H.; Arun, M. Effect of temperature on sedimentation stability and flow characteristics of magnetorheological fluids with damper as the performance analyser. *J. Magn. Magn. Mater.* **2022**, *555*, 169342. [CrossRef]
28. Rabbani, Y.; Ashtiani, M.; Hashemabadi, S.H. An experimental study on the effects of temperature and magnetic field strength on the magnetorheological fluid stability and MR effect. *Soft Matter* **2015**, *11*, 4453–4460. [CrossRef] [PubMed]
29. Choi, S.-B. Thermal Conductivity and Temperature Dependency of Magnetorheological Fluids and Application Systems—A Chronological Review. *Micromachines* **2023**, *14*, 2096. [CrossRef]
30. Roupec, J.; Berka, P.; Mazůrek, I.; Strecker, Z.; Kubík, M.; Macháček, O.; Andani, M.T. A novel method for measurement of MR fluid sedimentation and its experimental verification. *Smart Mater. Struct.* **2017**, *26*, 107001. [CrossRef]
31. Madhavrao Desai, R.; Acharya, S.; Jamadar, M.-H.; Kumar, H.; Joladarashi, S.; Sekaran, S.R. Synthesis of magnetorheological fluid and its application in a twin-tube valve mode automotive damper. *Proc. Inst. Mech. Eng. Part L J. Mater. Des. Appl.* **2020**, *234*, 1001–1016. [CrossRef]
32. Patel, S.; Upadhyay, R.; Patel, D. Design optimization of magnetorheological brake using structural parameter: Evaluation and validation. *IOP Conf. Ser. Mater. Sci. Eng.* **2020**, *992*, 012004. [CrossRef]
33. Lo Sciuto, G.; Kowol, P.; Capizzi, G. Modeling and Experimental Characterization of a Clutch Control Strategy Using a Magnetorheological Fluid. *Fluids* **2023**, *8*, 145. [CrossRef]

34. Coon, A.; Yang, T.H.; Kim, Y.M.; Kang, H.; Koo, J.H. Application of magneto-rheological fluids for investigating the effect of skin properties on arterial tonometry measurements. *Front. Mater.* **2019**, *6*, 45. [CrossRef]
35. Acharya, S.; Kumar, H. Investigation of magnetorheological brake with rotor of combined magnetic and non-magnetic materials. *SN Appl. Sci.* **2019**, *1*, 997. [CrossRef]
36. Yang, C.; Sakai, T.; Yamada, T.; Song, Z.; Takemura, Y. Improvement of pulse voltage generated by wiegand sensor through magnetic-flux guidance. *Sensors* **2020**, *20*, 1408. [CrossRef]
37. Shixu, L.; Jing, Z.; Jun, L.; Jie, F.; Miao, Y.; Song, Q. Enhancing Effect of Fe3O4/Nanolignocelluloses in Magnetorheological Fluid. *Langmuir* **2021**, *37*, 7176–7184. [CrossRef]
38. Ranjan, P.; Balasubramaniam, R.; Jain, V.K. Analysis, design and synthesis of water-based magnetorheological fluid for CMMRF process. *J. Micromanuf.* **2018**, *1*, 45–52. [CrossRef]
39. Brown, E.; Forman, N.A.; Orellana, C.S.; Zhang, H.; Maynor, B.W.; Betts, D.E.; DeSimone, J.M.; Jaeger, H.M. Generality of shear thickening in dense suspensions. *Nat. Mater.* **2010**, *9*, 220–224. [CrossRef]
40. Felicia, L.J.; Philip, J. Effect of hydrophilic silica nanoparticles on the magnetorheological properties of ferrofluids: A study using opto-magnetorheometer. *Langmuir* **2015**, *31*, 3343–3353. [CrossRef]
41. Bica, I.; Liu, Y.D.; Choi, H.J. Physical characteristics of magnetorheological suspensions and their applications. *J. Ind. Eng. Chem.* **2013**, *19*, 394–406. [CrossRef]
42. Kim, M.W.; Han, W.J.; Kim, Y.H.; Choi, H.J. Effect of a hard magnetic particle additive on rheological characteristics of micro-spherical carbonyl iron-based magnetorheological fluid. *Colloids Surf. A Physicochem. Eng. Asp.* **2016**, *506*, 812–820. [CrossRef]
43. Sherman, S.G.; Powell, L.A.; Becnel, A.C.; Wereley, N.M. Scaling temperature dependent rheology of magnetorheological fluids. *J. Appl. Phys.* **2015**, *117*, 17C751. [CrossRef]
44. Ji, J.; Wu, X.; Tian, Z.; Xie, F.; Chen, F.; Li, H. A Novel Magnetorheological Fluid with High-Temperature Resistance. *Materials* **2023**, *16*, 4207. [CrossRef] [PubMed]
45. Wang, G.; Zhao, D.; Li, N.; Zeng, Y.; Han, S.; Ma, Y.; Dong, X.; Yu, R. Facile synthesis of hierarchically structured flower-like Fe3O4 microspheres for high-performance magnetorheological fluids. *J. Ind. Eng. Chem.* **2019**, *79*, 217–225. [CrossRef]
46. Wang, K.; Dong, X.; Li, J.; Shi, K.; Li, K. Effects of silicone oil viscosity and carbonyl iron particleweight fraction and size on yield stress for magnetorheological grease based on a new preparation technique. *Materials* **2019**, *12*, 1778. [CrossRef]
47. Tian, J.; Chen, M.; Liu, H.; Qin, B.; Cheng, J.; Sun, Y. Study on mechanism of improving efficiency of permanent-magnet small ball-end magnetorheological polishing by increasing magnetorheological fluid temperature. *Sci. Rep.* **2022**, *12*, 7705. [CrossRef]
48. Khajehsaeid, H.; Alaghehband, N.; Bavil, P.K. On the Yield Stress of Magnetorheological Fluids. *Chem. Eng. Sci.* **2022**, *256*, 117699. [CrossRef]
49. Dang, A.; Ooi, L.; Fales, J.; Stroeve, P. Yield Stress Measurements of Magnetorheological Fluids in Tubes. *Ind. Eng. Chem. Res.* **2000**, *39*, 2269–2274. [CrossRef]
50. Tang, X.; Zhang, X.; Tao, R.; Rong, Y. Structure-enhanced yield stress of magnetorheological fluids. *J. Appl. Phys.* **2000**, *87*, 2634–2638. [CrossRef]
51. Yoon, J.-Y.; Kang, B.-H.; Kim, J.-H.; Choi, S.-B. New control logic based on mechanical energy conservation for aircraft landing gear system with magnetorheological dampers. *Smart Mater. Struct.* **2020**, *29*, 084003. [CrossRef]
52. Sung, K.G.; Choi, S.B. Effect of an electromagnetically optimized magnetorheological damper on vehicle suspension control performance. *Proc. Inst. Mech. Eng. Part D J. Automob. Eng.* **2008**, *222*, 2307–2319. [CrossRef]
53. Fang, F.F.; Choi, H.J.; Jhon, M.S. Magnetorheology of soft magnetic carbonyl iron suspension with single-walled carbon nanotube additive and its yield stress scaling function. *Colloids Surf. A Physicochem. Eng. Asp.* **2009**, *351*, 46–51. [CrossRef]
54. Jang, D.S.; Liu, Y.D.; Kim, J.H.; Choi, H.J. Enhanced magnetorheology of soft magnetic carbonyl iron suspension with hard magnetic γ-Fe2O3 nanoparticle additive. *Colloid Polym. Sci.* **2015**, *293*, 641–647. [CrossRef]
55. Wereley, N.M.; Chaudhuri, A.; Yoo, J.-H.; John, S.; Kotha, S.; Suggs, A.; Radhakrishnan, R.; Love, B.J.; Sudarshan, T.S. Bidisperse magnetorheological fluids using Fe particles at nanometer and micron scale. *J. Intell. Mater. Syst. Struct.* **2006**, *17*, 393–401. [CrossRef]
56. Leong, S.A.N.; Mohd Samin, P.; Idris, A.; Mazlan, S.A.; Rahman, A.H.A. Synthesis, characterization and magnetorheological properties of carbonyl iron suspension with superparamagnetic nanoparticles as an additive. *Smart Mater. Struct.* **2016**, *25*, 25025. [CrossRef]
57. Kim, B.G.; Yoon, D.S.; Kim, G.W.; Choi, S.B.; Tan, A.S.; Sattel, T. Design of a novel magnetorheological damper adaptable to low and high stroke velocity of vehicle suspension system. *Appl. Sci.* **2020**, *10*, 5586. [CrossRef]
58. Wilson, N.L.; Wereley, N.M.; Hu, W.; Hiemenz, G.J. Analysis of a magnetorheological damper incorporating temperature dependence. *Int. J. Veh. Des.* **2013**, *63*, 137. [CrossRef]